The Astronomical Journal, 169:48 (12pp), 2025 January https://doi.org/10.3847/1538-3881/ad9b1d

Resolving the Young 2 Cygni Runaway Star into a Binary Using iLocater

Justin R. Crepp[1], Jonathan Crass[1,2], Andrew J. Bechter[1], Brian L. Sands[1], Ryan Ketterer[1], David King[3,4], Derek Kopon[1], Randall Hamper[1], Matthew Engstrom[1], James E. Smous[1], Eric B. Bechter[1], Robert Harris[3], Marshall C. Johnson[2], Nicholas Baggett[1], Shannon Dulz[1], Michael Vansickle[1], Al Conrad[5], Steve Ertel[5,6], B. Scott Gaudi[2], Philip Hinz[6,7], Marc Kuchner[8], Manny Montoya[6], Eleanya Onuma[8], Melanie Ott[8], Richard Pogge[2], Gustavo Rahmer[5], Robert Reynolds[5], Christian Schwab[9], Karl Stapelfeldt[8,10], Joseph Thomes[8], Amali Vaz[6], Ji Wang (王吉)[2], and Charles E. Woodward[11]

[1] University of Notre Dame, Department of Physics and Astronomy, Notre Dame, IN, USA; jcrepp@nd.edu
[2] The Ohio State University, Department of Astronomy, Columbus, OH, USA
[3] Durham University, Department of Physics, Durham, UK
[4] University of Cambridge, Institute of Astronomy, Cambridge, UK
[5] Large Binocular Telescope Observatory, Tucson, AZ, USA
[6] University of Arizona, Department of Astronomy, Tucson, AZ, USA
[7] UC Santa Cruz, Department of Astronomy and Astrophysics, Santa Cruz, CA, USA
[8] Goddard Space Flight Center, Greenbelt, MD, USA
[9] Macquarie University, School of Mathematical and Physical Sciences, Sydney, NSW, Australia
[10] Jet Propulsion Laboratory, California Institute of Technology, Pasadena, CA, USA
[11] University of Minnesota, Minnesota Institute for Astrophysics, Minneapolis, MN, USA

Received 2024 August 30; revised 2024 December 05; accepted 2024 December 05; published 2024 December 24

Abstract

Precision radial velocity spectrographs that use adaptive optics (AO) show promise to advance telescope observing capabilities beyond those of seeing-limited designs. We are building a spectrograph for the Large Binocular Telescope (LBT) named iLocater that uses AO to inject starlight directly into single mode fibers. iLocater's first acquisition camera system (the SX camera), which receives light from one of the 8.4 m diameter primary mirrors of the LBT, was initially installed in summer 2019 and has since been used for several commissioning runs. We present results from first-light observations that include on-sky measurements as part of commissioning activities. Imaging measurements of the bright B3IV star 2 Cygni ($V = 4.98$) resulted in the direct detection of a candidate companion star at an angular separation of only $\theta = 70$ mas. Follow-up AO measurements using Keck/NIRC2 recover the candidate companion in multiple filters. An $R \approx 1500$ miniature spectrograph recently installed at the LBT named Lili provides spatially resolved spectra of each binary component, indicating similar spectral types and strengthening the case for companionship. Studying the multiplicity of young runaway star systems like 2 Cygni (36.6 ± 0.5 Myr) can help to understand formation mechanisms for stars that exhibit anomalous velocities through the Galaxy. This on-sky demonstration illustrates the spatial resolution of the iLocater SX acquisition camera working in tandem with the LBT AO system; it further derisks a number of technical hurdles involved in combining AO with Doppler spectroscopy.

Unified Astronomy Thesaurus concepts: Exoplanets (498)

1. Introduction

Radial velocity (RV) spectrographs have traditionally been installed on seeing-limited telescopes, or telescope ports that do not correct for atmospheric turbulence (D. A. Fischer et al. 2016). This design decision restricts spatial resolution, which in turn places practical limitations on spectral resolution. The ability to measure precise Doppler shifts is predicated on the quality, compactness, and signal-to-noise ratio of delivered images (E. B. Bechter et al. 2021). On a large telescope, adaptive optics (AO) improves spatial resolution by an order of magnitude relative to typical seeing conditions (100 mas versus 1000 mas). Thus, diffraction-limited imaging not only enhances both spatial and spectral resolution, but also enables the use of smaller core fibers—including those that propagate only a single spatial mode. This latter effect reduces the size of the instrument, allowing for the use of intrinsically stable materials that improve thermal stability, while eliminating fiber modal noise entirely (J. G. Robertson & J. Bland-Hawthorn 2012; C. Schwab et al. 2012; J. R. Crepp 2014).[12]

Of particular concern are Doppler uncertainties introduced by stellar absorption line asymmetries (H. M. Cegla et al. 2013, 2018, 2019). Subtle changes in the line profiles of stellar spectra are caused by surface inhomogeneities (spots, plage, faculae, granulation, etc.). These higher-order, time-dependent, and wavelength-dependent variations can only be measured at spectral resolutions above $R \approx 150{,}000$ at high signal-to-noise ratio (K. G. Strassmeier et al. 2015; A. B. Davis et al. 2017). The most stable and precise RV spectrographs are limited by such effects (X. Dumusque et al. 2014; P. Plavchan et al. 2015; X. Dumusque 2018; J. Crass et al. 2021b).

Spatial resolution also impacts the type of science cases that can be pursued. For example, unwanted spectral contamination from an unresolved binary or unrelated background star can cause large systematic errors that vary in time, even when using optical fibers (J. T. Wright et al. 2013). As a result, ground-based

---

[12] See A. J. Bechter et al. (2020) for a discussion of polarization noise.

exoplanet studies have primarily concentrated on observations of single stars to date. Overcoming this observational bias to study multistar systems would help challenge and substantiate theoretical models of planet formation and evolution (M. Moe et al. 2019).

Follow-up observations of transiting planets discovered from space missions like Kepler and TESS would also benefit from diffraction-limited RV spectroscopy (W. J. Borucki et al. 2013; G. R. Ricker et al. 2015). Unresolved binaries modify the radius and density estimates of transiting planets (S. B. Howell et al. 2012; D. R. Ciardi et al. 2013; M. E. Schwamb et al. 2013; E. B. Bechter et al. 2014; J. D. Eastman et al. 2016). Further, in the case of resolved binaries or chance-aligned background stars, uncertainty can remain regarding which star hosts which planet(s) (T. D. Morton et al. 2016).

iLocater is a diffraction-limited Doppler spectrograph being developed for the Large Binocular Telescope (LBT; J. R. Crepp et al. 2016). The instrument receives an AO-corrected beam and injects starlight directly into single mode fibers (SMFs), one for each 8.4 m diameter primary mirror plus a calibration fiber (A. Bechter et al. 2016; A. J. Bechter et al. 2020; J. Crass et al. 2021a). By achieving high spatial and spectral resolution simultaneously, iLocater shows promise to study planets in close-separation binaries. It will also advance our understanding of the masses, densities, orbits, and spin–orbit alignment of transiting planets, particularly around late-type stars (E. B. Bechter et al. 2019a, 2019b). For general astrophysics, the instrument may further be used to study the solar neighborhood involving crowded fields (young stellar cluster dynamics); weak absorption lines (composition of low-metallicity stars); line blanketing (substellar object atmospheric observations); and other applications (J. R. Crepp et al. 2016).

iLocater will use two separate acquisition camera systems, SX (left) and DX (right), to acquire light collected from each LBT primary mirror. Following delivery of hardware and confirmation of laboratory performance, the first iLocater acquisition camera system (SX) and fiber injection system was installed on the telescope in 2019 June. Daytime engineering activities allowed for coalignment to the LBT Interferometer system, which provides an AO-corrected beam to the instrument from the Single-conjugate AO Upgrade for the LBT (P. M. Hinz et al. 2016; E. Pinna et al. 2016). Further details of the SX acquisition camera design and technical engineering results can be found in J. Crass et al. (2021a). Once the remaining instrument modules are commissioned, forthcoming observations will use both the SX and DX acquisition cameras (J. Crass et al. 2022). The light will be coupled into two different SMFs, one located at each AO port (and a third fiber for calibration), allowing for simultaneous collection of spectra from closely separated sources using the same spectrograph (A. J. Bechter et al. 2020; J. Crass et al. 2022).

The star 2 Cygni was observed in 2019 July as part of first-light experiments from the commissioning of iLocater's SX acquisition camera. 2 Cygni has an elevated Gaia renormalized unit weight error (RUWE) value of 1.468, suggesting that it may be a multistar system (V. V. Makarov & G. H. Kaplan 2005; Gaia Collaboration et al. 2021). Serendipitously observed as a nearby bright star to diagnose hardware, imaging observations in the near-infrared (NIR; $\lambda = 0.927$–$0.960\ \mu$m) using the LBT AO system spatially resolved 2 Cygni into two distinct components. The very small measured angular separation of 70 mas ($\theta \approx 3\ \lambda/D$) suggests that the candidate may be a companion star. Follow-up imaging using Keck AO in 2022 July and spectroscopy using the Lili instrument at LBT in 2024 May corroborate the hypothesis that 2 Cygni may be a stellar binary system. These LBT commissioning observations demonstrate a key capability of the iLocater instrument, which is designed to operate at the diffraction limit.

Table 1
Observational Properties of the 2 Cygni System

Parameter	Value	Units	Reference
R.A.	19 24 07.58	hh:mm:ss	Gaia EDR3
Decl.	+29 37 16.81	deg:mm:ss	Gaia EDR3
$\mathrm{PM}_{\mathrm{R.A.}}$	12.235 ± 0.101	mas yr^{-1}	Gaia EDR3
$\mathrm{PM}_{\mathrm{decl.}}$	11.229 ± 0.123	mas yr^{-1}	Gaia EDR3
π	3.6239 ± 0.1362	mas	Gaia EDR3
U	4.16	mag	B. C. Reed (2003)
B	4.851 ± 0.014	mag	E. Høg et al. (2000)
V	4.977 ± 0.009	mag	Gaia DR3
G	4.932 ± 0.003	mag	E. Høg et al. (2000)
J	5.151 ± 0.017	mag	R. M. Cutri et al. (2003)
H	5.270 ± 0.033	mag	R. M. Cutri et al. (2003)
K	5.281 ± 0.021	mag	R. M. Cutri et al. (2003)

Note. Gaia Early Data Release 3 (EDR3) is from the Gaia Collaboration et al. (2021).

In this paper, we describe the literature surrounding 2 Cygni (Section 2); commissioning observations that resolve 2 Cygni for the first time, Keck/NIRC2 follow-up imaging, and direct spectroscopic measurements (Section 3); the modular data analysis pipeline developed for iLocater's acquisition camera systems (Section 4); and results from astrometric, photometric, spectroscopic, and other analyses (Section 5). Concluding remarks are provided in Section 6.

2. 2 Cygni Background

2 Cygni is a naked-eye star system ($V = 4.98$), with Table 1 listing its observational properties. 2 Cygni is identified as a binary in the Catalog of Components of Double and Multiple stars (CCDM) by J. Dommanget & O. Nys (2002), with original discoverer "WRH" (R. H. Wilson). However, R. H. Wilson (1950) identifies the star as a "single." Further, the components of 2 Cygni are listed as being separated by 1.″58 in R.A. and 16.″8 in decl. At the distance of 2 Cygni (d = 276 ± 11 pc), this separation corresponds to 8000 au in projection, raising questions about their association. Our observations reveal a companion star at $\theta = 70$ mas that remains to be explained. The neighboring star listed in CCDM at 29″ separation may be aligned by chance and was outside of the field of view of both iLocater and follow-up NIRC2 AO imaging.

A further interest in the 2 Cygni system is its nature as a young (36.6 ± 0.5 Myr) runaway star: N. Tetzlaff et al. (2011) characterize 2 Cygni as a runaway star with a peculiar velocity of 22.9 ± 2.9 km s^{-1} (19.4 km s^{-1} tangential to the sky). This speed places it above the peak in the measured three-dimensional space velocity histogram of peculiar stars. Studying the multiplicity of runaway star systems can help to distinguish between event scenarios thought to explain their existence, such as binary supernovae and dynamical ejection from dense young clusters (A. Blaauw 1961; A. Poveda et al. 1967).

2 Cygni is also known as HD 182568, HIP 95372, HR 7372, SAO 87159, GC 26785, BD+293584, CCDM J19241+2937AB, and 2MASS J19240757+2937169. 2 Cygni has been identified as

a probable, long-period astrometric binary by C. Turon et al. (1993), J. Dommanget & O. Nys (2002), R. Wielen et al. (2000), and P. P. Eggleton & A. A. Tokovinin (2008). However, its true multiplicity is currently unknown.

The Gaia DR3 archive shows an RUWE value of 1.468 for 2 Cygni, suggesting that the observed motion and point-spread function (PSF) fitting procedure creates potential problems with a standard astrometric solution for a single star, but the "non-single-star" flag is set to zero (Gaia Collaboration et al. 2021). The Hipparcos Input Catalog (HIC) lists two components, but no astrometric binary flag or any further notes on the source (C. Turon et al. 1993). Based on available documentation, this information was likely obtained from the CCDM. The Hipparcos Catalog (M. A. C. Perryman et al. 1997) shows a flag of "system previously identified as multiple in HIC," but then lists only one component, as does the update in 2007 (F. van Leeuwen 1993). The R. Wielen et al. (2000) FK6 catalog lists 2 Cygni with flags "RV may be variable, or composite spectrum or other weak indications of binary or suspected planet" and "delta mu binary" from proper motion differences.

P. P. Eggleton & A. A. Tokovinin (2008) use a number of catalogs to list multiplicities of Hipparcos stars. 2 Cygni (HR 7372) has an "estimated most probable multiplicity" of $n = 2$ with a flag stating "is for an entry that has been identified as a probable astrometric binary by MK, ..." MK refers to V. V. Makarov & G. H. Kaplan (2005) who lists "2Cyg" in their table of "A catalog of astrometric binaries with discrepant proper motions in Hipparcos and Tycho-2," but not in their table of "A catalog of astrometric binaries with accelerating proper motions in Hipparcos."

In an attempt to identify calibration stars for optical interferometers, S. J. Swihart et al. (2017) attempt to weed out known binaries using P. P. Eggleton & A. A. Tokovinin (2008), but leave in "2Cyg." P. P. Eggleton & A. A. Tokovinin (2008) provide a cross-link to the D. Hoffleit & C. Jaschek (1991) Bright Star Catalogue, which lists 2 Cygni (HR 7372) as a multiple with a flag that says it was identified by "Worley (1978) update of the IDS" and also leaves the Aitken's Double Star catalog value blank. We assume the "Worley (1978) update to the IDS" refers to C. E. Worley (1978) but are unable to locate 2 Cygni in the Worley report.

CCDM by J. Dommanget & O. Nys (2002) lists two components to the 2 Cygni system. Component B has the discover listed as "WRH." WRH references "discoverer codes" in the Washington Double Star catalog C. E. Worley & G. G. Douglass (1997), which lists 13 R. H. Wilson papers plus one unpublished manuscript. However, only one of these papers, R. H. Wilson (1950), explicitly lists 2 Cygni, stating that it is a "single" instead of listing component separations as with other targets.

Table 2 lists relevant references that informed our literature search. We have checked the Keck, Gemini, MMT, ESO, and NAOJ data archives but did not find AO imaging data of 2 Cygni. To our knowledge, 2 Cygni has not been observed with AO using a large telescope and the true multiplicity of the system is currently unknown.

Table 2
Select Literature References That Mention 2 Cygni

Reference	Comments
R. H. Wilson (1950)	single star
D. Hoffleit & C. Jaschek (1991)	multiple star with reference to C. E. Worley (1978)
C. Turon et al. (1993)	two components
C. E. Worley & G. G. Douglass (1997)	discoverer codes referenced by J. Dommanget & O. Nys (2002)
M. A. C. Perryman et al. (1997)	one component
R. Wielen et al. (2000)	proper motion indicated binary
J. Dommanget & O. Nys (2002)	binary with discoverer "WRH"
V. V. Makarov & G. H. Kaplan (2005)	astrometric binary with discrepant proper motion
P. P. Eggleton & A. A. Tokovinin (2008)	probable multiplicity of two; reference to V. V. Makarov & G. H. Kaplan (2005)
S. J. Swihart et al. (2017)	assumes 2 Cygni is single
Gaia Collaboration et al. (2021)	RUWE = 1.468
This Paper	2 Cygni resolved into binary

3. Observations

3.1. Adaptive Optics Imaging

The 2 Cygni system was first observed by the iLocater SX acquisition camera system during instrument commissioning on UT 2019 July 9. Follow-up measurements were then obtained with Keck/NIRC2 AO on UT 2022 July 13 to corroborate the iLocater data. More recently, direct spectroscopic measurements were obtained using the Lili spectrograph at the LBT on UT 2024 May 17. Table 3 provides an observing log that summarizes the measurements. Images from each instrument are shown in Figures 1, 2, and 3.

3.1.1. iLocater Imaging

AO imaging observations were performed using iLocater's fine guiding camera (FGC). The FGC uses an Andor Zyla 4.2 Plus high-speed CMOS camera with 6.5 μm pixels (2048 × 2048 array). The FGC offers high frame rate imaging to acquire centroid data that help characterize residual vibrations, tip/tilt correction, and improve fiber coupling performance (A. J. Bechter et al. 2020; J. Crass et al. 2021a). Wavelengths in the narrow range $\lambda = 0.927$–0.960 μm are sent to the FGC through the combination of two dichroics, one for the AO system wave front sensor and another internal to the acquisition camera that diverts light to the spectrograph.

The SX FGC design offers a field of view of $8'' \times 8''$ with a plate scale of $0\farcs61 \pm 0\farcs08$ mm^{-1} (3.97 ± 0.52 mas pixel^{-1}). Images are by default recorded with a changing parallactic angle due to the binocular mounting of each telescope primary mirror. No internal K-mirror systems are used to compensate for field rotation. Instead, the changing parallactic angle is compensated for in software. This feature may be used in the future for high-contrast, angular differential imaging measurements to suppress speckles (C. Marois et al. 2008). A precise atmospheric dispersion corrector compensates for chromatic refraction to improve delivered imaging quality and maximize SMF injection efficiency into the spectrograph. Efforts to precisely calibrate the plate scale, FGC north–east orientation, and establish rotation angle relations are ongoing. Further details of the SX acquisition camera system design and commissioning activities are described in J. Crass et al. (2021a).

3.1.2. NIRC2 Imaging

Follow-up measurements using NIRC2 consisted of a sequence of undithered NIR exposures in position angle mode

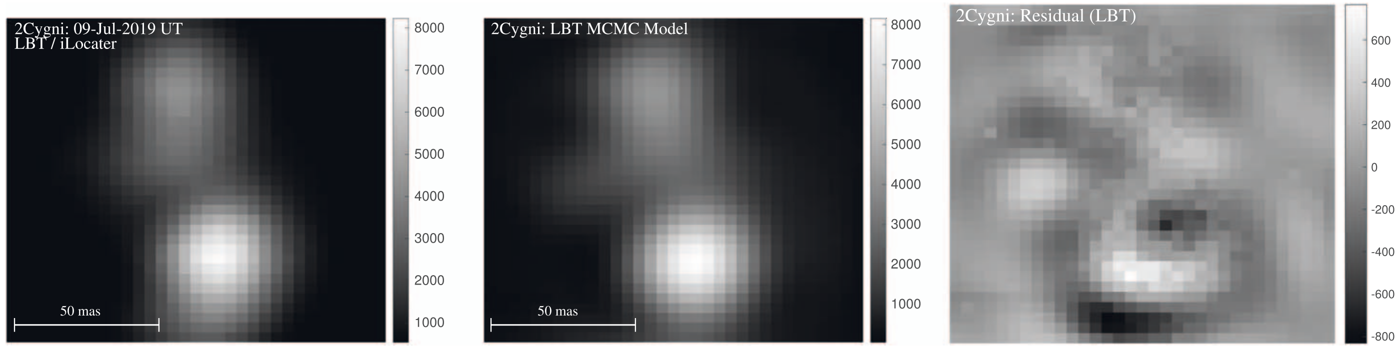

Figure 1. Discovery image recorded with the iLocater SX acquisition camera system on 2019 July 9 (left), Markov Chain Monte Carlo (MCMC) model using Zernike polynomials (middle), and intensity residuals (right). North–east orientation has not been calibrated.

Table 3
Observing Log for Adaptive Optics Measurements of 2 Cygni

Date (UT)	Instrument	Filter	Mode	N_{frames}	Δt_{int} (s)	Δt_{tot} (s)	Airmass	θ ($''$)
2019 Jul 9	iLocater SX	custom	Imaging	100	0.11	11	1.10	0.9
2022 Jul 13	NIRC2	H_{cont}	Imaging	20	10.56	211.2	1.06	0.6
2022 Jul 13	NIRC2	K_{cont}	Imaging	10	10.56	105.6	1.06	0.6
2024 May 17	Lili	custom	Spectroscopy	100	0.5	50.0	1.02	0.7–1.0
2024 May 17	iLocater SX	custom	Imaging	1000	0.11	110	1.02	0.7–1.0

Note. iLocater's custom imaging channel senses light within a narrow range of wavelengths ($\lambda = 0.927$–$0.960\ \mu$m). The number of frames (N_{frames}), integration time per frame (Δt_{int}), and total integration time (Δt_{tot}) are shown for each data set. Seeing measurements (θ) were made using the LBT DIMM system (within 25° of the target) and Keck MASS/DIMM system.

using the Keck II AO system. A subarray mode of 512×512 pixels was used to offer short integration times. Given the extreme brightness of 2 Cygni, the K_{cont} and H_{cont} filters were used to avoid saturation. The candidate companion star was recovered in both data sets (Figures 2, 3). Since observations of 2 Cygni occurred during execution of another scientific program, no PSF calibration stars were observed. Images were processed using standard techniques for interpolation of hot pixel values, flat-fielding, and precise image combination (J. R. Crepp et al. 2014). Photometric and astrometric analysis was performed on the combined images from each filter.

3.2. Spectroscopy

2 Cygni was observed using a miniature spectrograph named Lili, which stands for “Little iLocater,” that we recently installed at the LBT as part of an experiment to characterize the end-to-end performance of the iLocater light path (R. J. Harris et al. 2024). Lili covers the iLocater spectral passband ($\lambda = 0.97$–$1.31\ \mu$m) with a resolving power of $R \approx 1500$ at a sampling of 2 pixels per resolution element. As Lili is a test spectrograph, only one hardware mode is available: a triple-stacked volume phase holographic grating provides access to two spectral orders that are imaged onto a C-RED 2 camera. The C-RED 2 detector is liquid cooled to −40 °C to minimize dark current. See R. J. Harris et al. (2024) for further information on Lili.

The 2 Cygni system was observed during twilight on UT 2024 May 17 at an elevation of approximately 85°; 100 frames were recorded for 2 Cygni A and 2 Cygni B each. Seeing was estimated with the LBT DIMM to vary between 0.″7 and 1.″0. During observations, the detector gain was set to high with an integration time of 0.5 s. Data were recorded using the First Light Vision Software program and saved in .fits format. With the target being resolved by the SX acquisition camera, the instrument SMF was accurately aligned to each stellar component separately using the fiber back-illumination method described in J. Crass et al. (2021a). Significant care was taken to avoid spectral cross contamination between the two sources; the iLocater SX acquisition camera is capable of centering and maintaining fiber alignment to within ≈10 mas, a small fraction of the $\theta = 97 \pm 9$ mas angular separation of the sources during the 2024 May observing run (A. J. Bechter et al. 2020).

4. Data Analysis

4.1. Imaging Pipeline

We have developed a semiautomated reduction pipeline that analyses AO imaging data recorded by iLocater's SX acquisition camera system. The software design is modular so that it can also handle data acquired from the DX acquisition camera system in the future. The pipeline preprocesses (prepares images, files, and directories), cleans (pixel intensity outliers), calibrates (flat-fielding and background subtraction), and derotates, aligns, and combines images recorded through an observing sequence. The pipeline is written in MATLAB and uses methods similar to that of the TRENDS high-contrast imaging program developed for the NIRC2 instrument at Keck (J. R. Crepp et al. 2012, 2013, 2014).

Images are first collated and conditioned based on user-defined input values that specify working directories and ancillary information about the data set. Uploaded files are made available for the user to qualitatively assess AO correction and select frames. Standard methods are used for background subtraction, hot pixel cleaning, flat-fielding, etc.

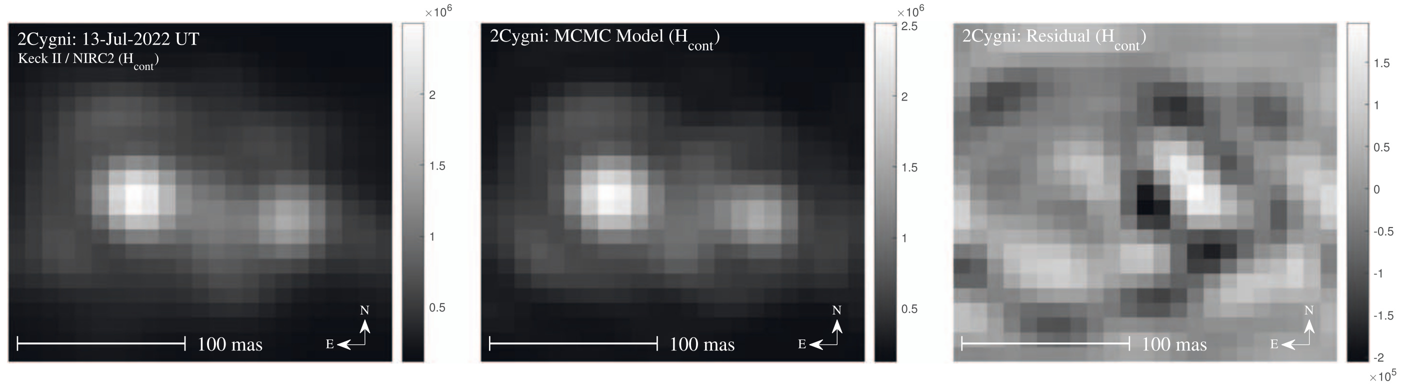

Figure 2. High resolution follow-up images of 2 Cygni taken in the H_{cont} filter using Keck/NIRC2. The three panels show the processed data (left), MCMC model (middle), and intensity residuals (right).

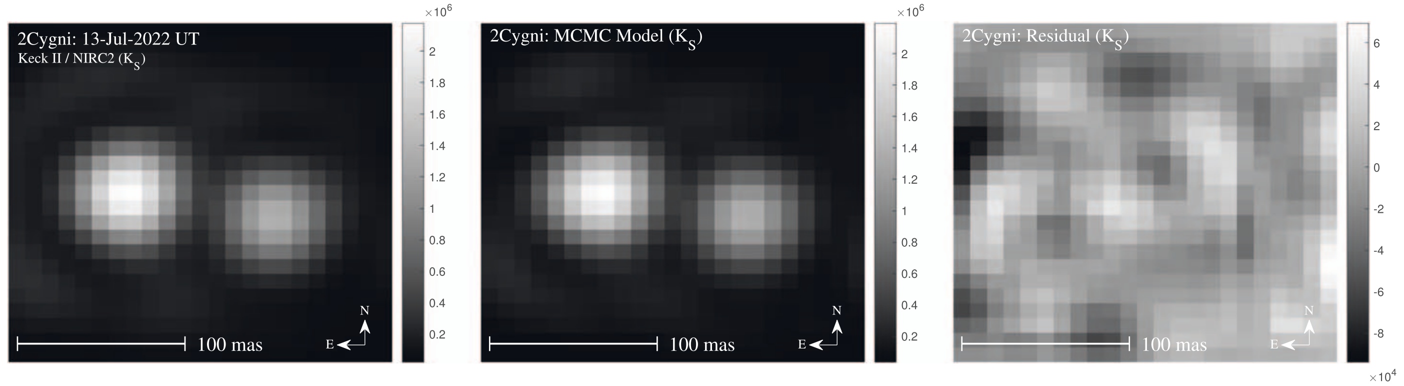

Figure 3. High resolution follow-up images of 2 Cygni taken in the K_s filter using Keck/NIRC2. The three panels show the processed data (left), MCMC model (middle), and intensity residuals (right).

Telemetry from the telescope control system is used to orient frames based on the evolving parallactic angle throughout the course of an observing sequence. Frames are then coaligned using a Fourier method that is accurate to the subpixel level (M. Guizar-Sicairos et al. 2008; J. R. Crepp et al. 2011; L. Pueyo et al. 2012). Finally, the frames are median combined to prepare for analysis. Future versions of the pipeline will incorporate the ability to perform angular differential imaging to search for companions that may be initially hidden by speckle noise.

4.2. Point-spread Function Fitting

Contamination from the constituent PSFs of closely separated stars can bias the interpretation of photometry and astrometry data. Given that the angular separation of the 2 Cygni binary is comparable to the diffraction-limited spatial resolution of the LBT AO system, we did not attempt aperture photometry. Instead, a Bayesian statistical method was developed and used to account for overlapping PSFs and self-consistently extract relative photometry and astrometry information. The method is similar to E. B. Bechter et al. (2014), except that the PSFs are fitted using a physics-based model of aberrations.

We developed an imaging model to fit intensity measurements obtained for each (aligned and median-combined) AO data set. MCMC computations were used to explore the model fit parameter space by numerically calculating a likelihood function for a given set of variables. The Metropolis–Hastings algorithm was implemented to find optimal model parameters and create posterior distributions in order to derive rigorous uncertainties (N. Metropolis et al. 1953; W. K. Hastings 1970).

A Bayesian likelihood function, $\mathcal{L}(\phi)$, is constructed based on model parameters $\phi(x_j, y_j, F_j, S, \ldots)$ that include centroid positions (x_j, y_j), peak intensity values (F_j), the sky background (S), and several nuisance parameters which are described below. The index $j = \{1, 2, \ldots\}$ represents each individual star (binary in this case). The likelihood function is evaluated by comparing the intensity of the model at each pixel i to recorded images at the same pixel,

$$\mathcal{L}(\phi) = \Pi_i \quad (2\pi\sigma_i^2)^{-1/2} \quad \exp\left(-\frac{\Delta I_i(\phi)^2}{2\sigma_i^2}\right), \tag{1}$$

where the uncertainty in the measured intensity, σ_i, is assumed to be dominated by photon noise and given by a Poisson distribution, which we approximate as Gaussian.

Using the Metropolis–Hastings algorithm, we compute the natural logarithm of the likelihood to explore the high-dimensional parameter space of model variables and avoid numerical precision limitations,

$$\ln \mathcal{L}(\phi) = -\frac{1}{2}\sum_i (\ln(2\pi\sigma_i^2) + \Delta I_i(\phi)^2/\sigma_i^2). \tag{2}$$

The quantity $\Delta I_i(\phi) = I_{\mathrm{model}_i}(\phi) - I_{\mathrm{data}_i}$ is found by evaluating the intensity contributed by each star in addition to the sky background,

$$I_{\mathrm{model}_i}(\phi) = I_{i,j=1} + I_{i,j=2} + S, \tag{3}$$

where S is assumed to be constant over the narrow field of view of iLocater.

To account for imperfect AO correction, we model the PSF of each star to accommodate aberrations that would otherwise distort and bias the astrometric and photometric solutions. Given the small angular separation of the 2 Cygni components, we assume isoplanatic conditions: light from each star experiences the same turbulence upon arriving to the telescope and therefore the PSFs are essentially identical. We model both PSFs simultaneously using fully reduced images.

It is assumed that (quasi-)static aberrations dominate the PSF for integrations significantly longer than an AO cycle. Thus, an optical model that includes low-order aberrations was used to fit each stellar PSF. The central obstruction relative diameter of the LBT and Keck were included to model diffraction for each telescope. The first 14 Zernike polynomials (excluding piston and tip and tilt) were superposed in the pupil plane to create a wave front phase aberration. This number of free parameters strikes a good balance between model accuracy and computational load. Uniform priors were assumed for all Zernike coefficients over an allowable range of (−1, −1). Uncertainties in fitted parameters are given by 68% confidence intervals derived from posterior distributions.

After using a Markov process to create a phase shape, incorporating the telescope central obstruction, the resulting electric field was then propagated to the image plane using a Fourier transform. Taking the square modulus of the image plane field, the resulting intensity pattern was then duplicated to create two identical stellar PSFs. Different centroid positions, equivalent to tip and tilt variables in the pupil plane, were applied using the Fourier shift theorem. The peak flux of each binary component was applied as a multiplicative factor. On-sky images were truncated to a narrow field of view so that the MCMC algorithm could efficiently explore the stellar PSFs. All free parameters were marginalized over when calculating posterior values.

Following an initial estimate for each free parameter, the MCMC routine was run to find a global minimum for the modeled image. Several million additional iterations were then performed to mix the MCMC chain, explore the parameter space surrounding the global minimum, and create well-sampled posterior distributions. Algorithm convergence was assessed using the Gelman–Rubin criteria by comparing the variance of the chain to the mean value for each parameter (A. Gelman & D. B. Rubin 1992).

4.3. Spectroscopy with Lili

Data reduction and calibration of Lili measurements followed the steps described in R. J. Harris et al. (2024), which we briefly summarize. A custom Python program based on the optimal extraction technique of K. Horne (1986) was developed to rotationally interpolate and extract spectra from the two raw spectral orders measured by Lili. A halogen lamp was used to define the spectral profile. A wavelength solution was computed based upon an Ar lamp spectrum. Gaussian fits were used to measure absorption line centroids and a quadratic fit produced the dispersion solution for each order. The resulting wavelength solution achieved an rms of 0.05 nm or better. The spectra were continuum normalized using a spline fit, excluding regions affected by tellurics or strong stellar lines. A barycentric correction was applied using the Astropy library to Doppler shift wavelength features based on Earth's motion around the Sun relative to 2 Cygni.

Observations of Vega and Arcturus were used to help validate the on-sky measurements recorded for 2 Cygni. However, because the observations were conducted during a shared-risk mode (engineering time) with a new instrument, we were unable to observe a telluric reference of similar spectral type in the same part of the sky at the same time as 2 Cygni; thus the spectra have not been corrected for telluric features. Nevertheless, we are able to use the spatially resolved spectra to compare each stellar component to one another, as well as to theoretical atmospheric models, in an effort to classify spectral types and constrain the effective temperature and surface gravity.

5. Results

5.1. Photometry and Astrometry

Figures 1, 2, and 3 show model images of 2 Cygni compared to data obtained for each observing configuration. Differenced image residuals have rms values of 2.3%, 2.4%, and 1.2% for the iLocater data (33 × 33 pixels) and Keck $H_{\rm cont}$ and $K_{\rm cont}$ data (22 × 22 pixels), respectively, indicating a good fit using the MCMC method (Section 4.2). We use results from the PSF fitting procedure to analyze the relative photometry and astrometry of the candidate companion. Figure 4 shows a more recent AO image of 2 Cygni from 2024 May. Figure 5 shows contrast curves for each iLocater AO imaging epoch.

Since 2 Cygni does not have a Y-band NIR measurement in the literature to our knowledge, and the iLocater camera system uses a custom filter, we deblend the photometry of 2 Cygni's combined light signal using the NIRC2 measurements. Apparent and absolute magnitudes of each source (A, B) are estimated in the H and K_s bands (Table 4). Apparent magnitudes are given by,

$$m_A = m_{AB} + 2.5\log_{10}(1 + f_B/f_A), \quad (4)$$

$$m_B = m_{AB} + 2.5\log_{10}(1 + f_A/f_B), \quad (5)$$

where m_{AB} is the total system apparent magnitude and f_A and f_B are the relative flux of each source. Given the extreme brightness of the 2 Cygni system, we had to use $H_{\rm cont}$ and $K_{\rm cont}$ filters with NIRC2 AO observations to avoid saturation. Thus, the photometry analysis should be considered as an estimate only, interpreted with the caveat that the $H_{\rm cont}$ and $K_{\rm cont}$ measurements were used as a proxy in the absence of broadband H and K_s data.

Assuming that the candidate companion is associated with 2 Cygni (see Sections 5.2 and 5.3), we calculate absolute magnitudes for the primary and secondary source accounting for the combined light signal (Table 4). An H-R diagram of the 2 Cygni components is shown in Figure 6. 2 Cygni B appears to be near the main sequence in close proximity to 2 Cygni A, with both components being early-type stars.

We note that the multiplicity fraction (binaries plus higher-order multiples) of B-type stars exceeds ≈80% and that the distribution is roughly flat with semimajor axis when plotted on a logarithmic scale (e.g., Öpik's law; S. S. R. Offner et al. 2023). Using the absolute magnitudes of each component, we estimate individual masses of $M_A = 6.85 \pm 0.15\ M_\odot$ and $M_B = 5.90 \pm 0.18\ M_\odot$ using solar-metallicity isochrones from L. Girardi et al. (2002) evaluated at an age of 35 Myr. These values are derived as a weighted average using the mass of each component estimated from individual H- and K_s-band

Table 4
Deblended Photometry for the 2 Cygni Components Using NIRC2

Star	m_H	m_{K_s}	M_H	M_{K_s}	$H - K_s$
2 Cygni A	5.765 ± 0.069	5.782 ± 0.043	−1.439 ± 0.108	−1.422 ± 0.094	−0.017 ± 0.082
2 Cygni B	6.360 ± 0.071	6.361 ± 0.044	−0.844 ± 0.110	−0.843 ± 0.095	−0.001 ± 0.085

Note. H-band data are based on $H_{\rm cont}$ measurements and K_s-band data are based on $K_{\rm cont}$ measurements.

Table 5
2 Cygni Astrometry Showing the Angular Separation (ρ), Position Angle Measured East of North, and Magnitude Difference in the iLocater Filter

Instrument	Epoch	ρ (mas)	PA (deg)	Δm
iLocater	2019 Jul 9	70 ± 9	⋯	0.66 ± 0.10
NIRC2	2022 Jul 13	91 ± 1	261.1 ± 0.4	Table 4
iLocater	2024 May 17	97 ± 9	⋯	0.54 ± 0.10

Note. The uncertainty in the angular separation from the iLocater astrometry measurements is dominated by the uncertainty in the plate scale. The calibration of iLocater's north–east orientation with changing parallactic angle is ongoing. The position angle (PA) is shown in the fourth column.

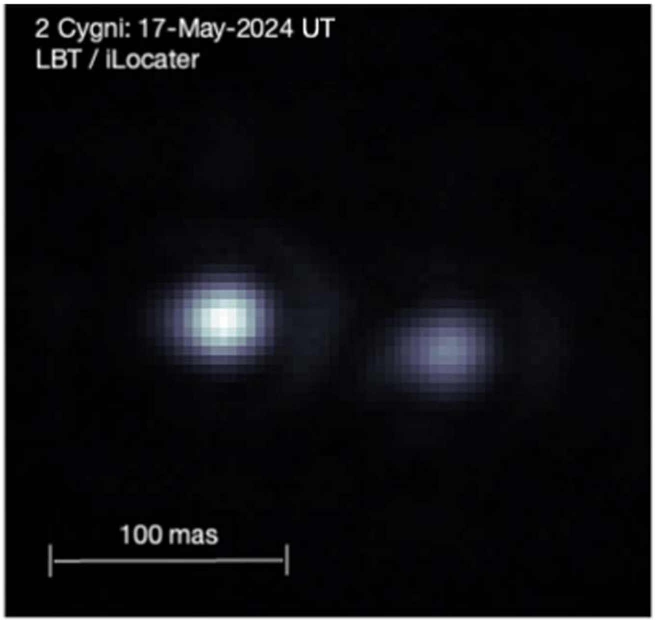

Figure 4. Processed AO image of 2 Cygni from the iLocater SX acquisition camera system recorded in 2024 May.

photometry. Such a high mass ratio, $q = M_B/M_A = 0.86 \pm 0.06$, is fairly uncommon for early-type binary stars, which show a peak in the distribution of $q \approx 0.3$ (K. Gullikson et al. 2016; M. Moe & R. Di Stefano 2017).

Astrometric results from each instrument are shown in Table 5. Given that iLocater's north–east orientation is not yet calibrated, we estimate the maximum orbital motion that would be possible over a 4.85 yr astrometric baseline assuming an edge-on circular orbit. Conservatively using a total system mass of $M_{\rm tot} \approx 13\ M_\odot$ and semimajor axis (equal to the 2019 projected separation, 70 mas × 276 pc = 19.3 au), the shortest Keplerian orbital period is $P \approx 24$ yr. This motion on the sky corresponds to at most an ≈89 mas change in angular separation. Given that 2 Cygni's separation has changed by only 27 ± 13 mas over this time frame (Table 5), it is plausible that the two stars may be gravitationally associated. Meanwhile, the proper motion of 2 Cygni is ≈17 mas yr^{-1} corresponding to an 82 mas expected change in separation for an unrelated background source (Gaia Collaboration et al. 2021). Additional high resolution imaging data with calibrated

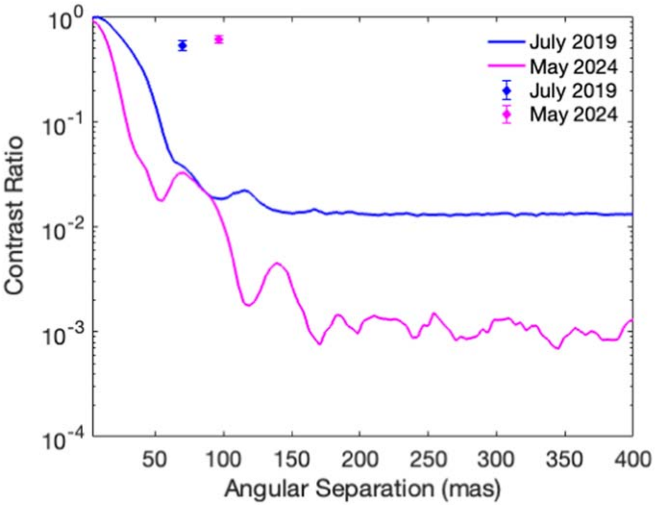

Figure 5. Contrast curves showing the achieved dynamic range for each AO imaging epoch using iLocater. A deeper exposure, lower airmass, and improved instrument calibration offer better contrast for the 2024 May observing run compared with 2019 July. The angular separation and flux ratio of 2 Cygni B is shown for reference.

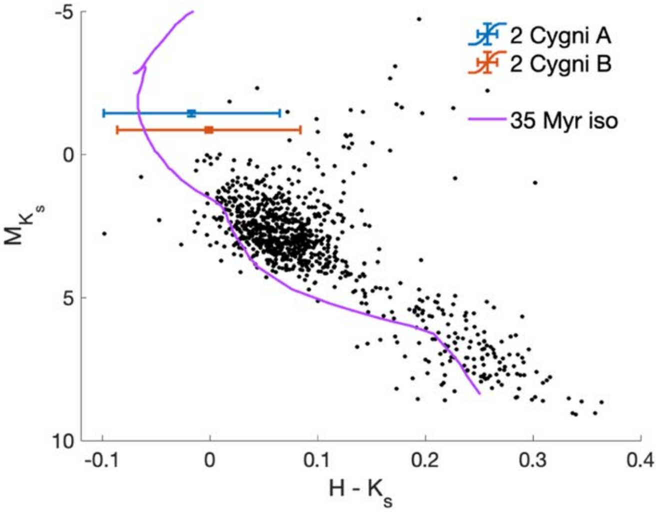

Figure 6. H-R diagram showing the 2 Cygni components. Overplotted are 1000 stars within 200 pc randomly drawn from the Two Micron All-Sky Survey (2MASS) catalog (R. M. Cutri et al. 2003). A solar-metallicity 35 Myr isochrone from L. Girardi et al. (2002) is shown for comparison.

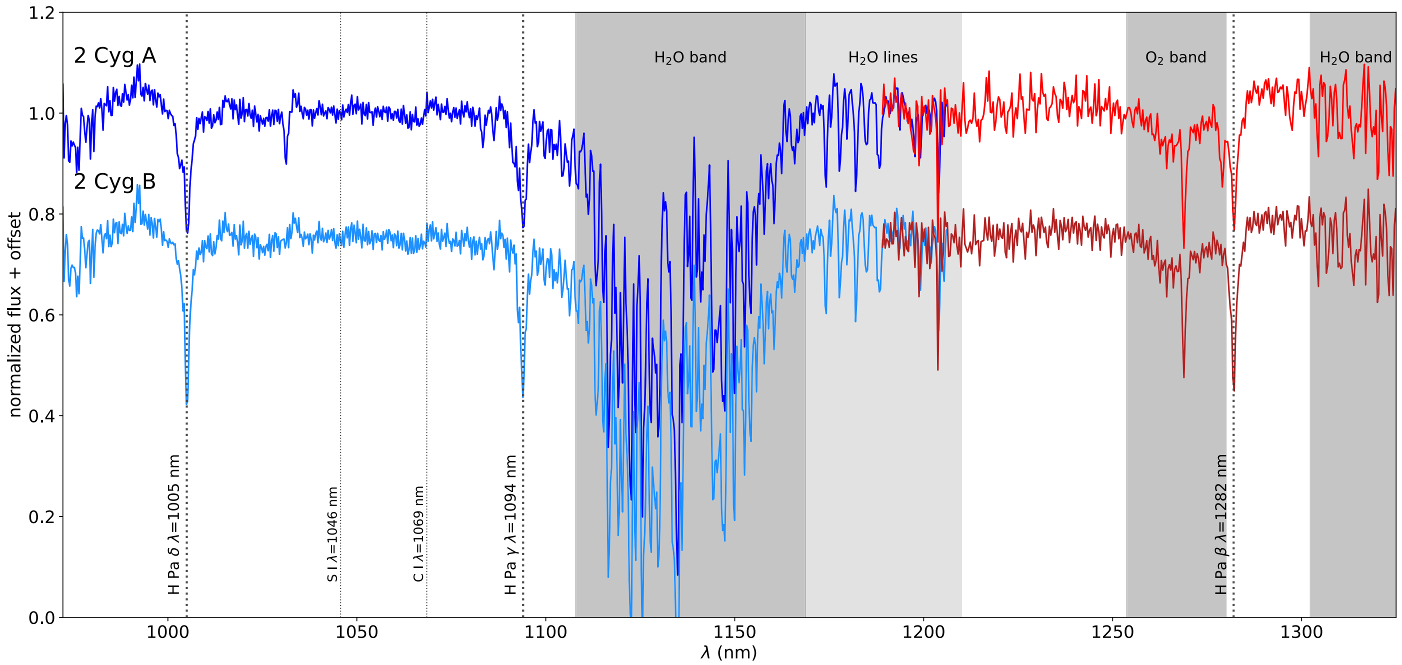

Figure 7. Spectra of the 2 Cygni A and B components recorded with the Lili spectrograph. Blue and red colors indicate the two measured orders. The two stars have comparable spectral types and show few absorption lines.

position angle measurements are required to more definitively assess companionship and attempt to distinguish orbital motion from proper motion and parallactic motion.

5.2. Spectral Characterization

Figure 7 shows a comparison of the low resolution spectra extracted for each 2 Cygni component. Blue curves represent the short wavelength order and red curves represent the long wavelength order. Major H_2O and O_2 telluric bands are indicated. Given the similar structure and features of the spectra, including a dearth of absorption lines, 2 Cygni B appears to have an early (B-type) spectral classification comparable to 2 Cygni A.

To estimate the possible spectral contamination experienced by the companion, we generate an AO imaging contrast curve. Contrast was estimated using 1σ intensity variations as a function of radial separation using the modeled PSF of 2 Cygni A with the candidate companion PSF removed. As shown in Figure 5, the expected contamination of 2 Cygni B spectra from the nearby 2 Cygni A primary was ≈3% ($\theta = 97 \pm 9$ mas) for the 2024 May run. Given the iLocater acquisition camera measured a brightness difference of $\Delta m \approx 0.54$ mag, the spatially resolved 2 Cygni B spectrum can be trusted to ≈5%. This level of systematic contamination is comparable to spectral variations resulting from not correcting for tellurics.

To further assess the nature of 2 Cygni A and B, we analyzed the Paschen series of NIR hydrogen absorption lines (Paδ, Paγ, and Paβ) as well as neutral helium (He I). Figure 8 shows each line following continuum normalization for effective temperatures ranging from $T_{\rm eff} = 10{,}000$ K to $T_{\rm eff} = 22{,}000$ K. For comparison, we overplot BT-Settl spectral models[13] for different effective temperatures assuming a surface gravity of $\log(g) = 4.0$ (F. Allard et al. 2011). For each hydrogen feature, we find that 2 Cygni B exhibits a deeper line depth indicating a cooler temperature than 2 Cygni A. Neutral helium corroborates this observation by demonstrating consistency through the opposite trend, whereby shallow line depths also point toward a lower temperature for 2 Cygni B.

As a more comprehensive analysis, we consider a range of surface gravities. Figure 9 shows BT-Settl model grid comparisons for the full measured spectrum and Figure 10 shows a line-by-line analysis (F. Allard et al. 2011). We estimate the uncertainties on the spectral data points using photon-counting statistics and the known gain and read noise of the detector, propagated forward through the data reduction process. A reduced chi-squared value is then computed for each model compared to the data, in a narrow window around each absorption line. The best-fitting range of stellar parameters is found from the regions where $\chi^2_{\rm red} < 1$.

At the resolution and sensitivity of the Lili measurements, we find that it is possible to discern effective temperatures whereas surface gravity is only loosely constrained. Paγ and Paδ features are well fit by theoretical models because they are strong lines without continuum normalization issues in the vicinity. For Paβ, the models are less well fit to absorption lines because the continuum normalization has more difficulty in order 2 (all of the other lines are in order 1) and the blaze efficiency drops rapidly at the end of the order. The He I line is shallow, only barely detected above the noise for 2 Cygni A and not significantly detected for 2 Cygni B.

Altogether, this analysis confirms that 2 Cygni B has a lower $T_{\rm eff}$ than 2 Cygni A. Meanwhile, model fits for 2 Cygni A prefer a higher surface gravity than 2 Cygni B but the results are marginal. Using the full spectrum, 2 Cygni A is most consistent with $T_{\rm A} \approx$ 16,000–20,000 K and $\log(g) \approx 3.75 - 4.75$, whereas 2 Cygni B is most consistent with $T_{\rm B} \approx$ 10,000–14,000 K and $\log(g) \approx$ 3.00–4.25. These effective temperatures correspond roughly to spectral types of B3–B4 and B6–B9, respectively (R. O. Gray & C. J. Corbally 1994), consistent with the combined light visible spectral classification of the 2 Cygni system of B3IV from SIMBAD, given that the signal is dominated at shorter

---

[13] http://svo2.cab.inta-csic.es/theory/newov2/

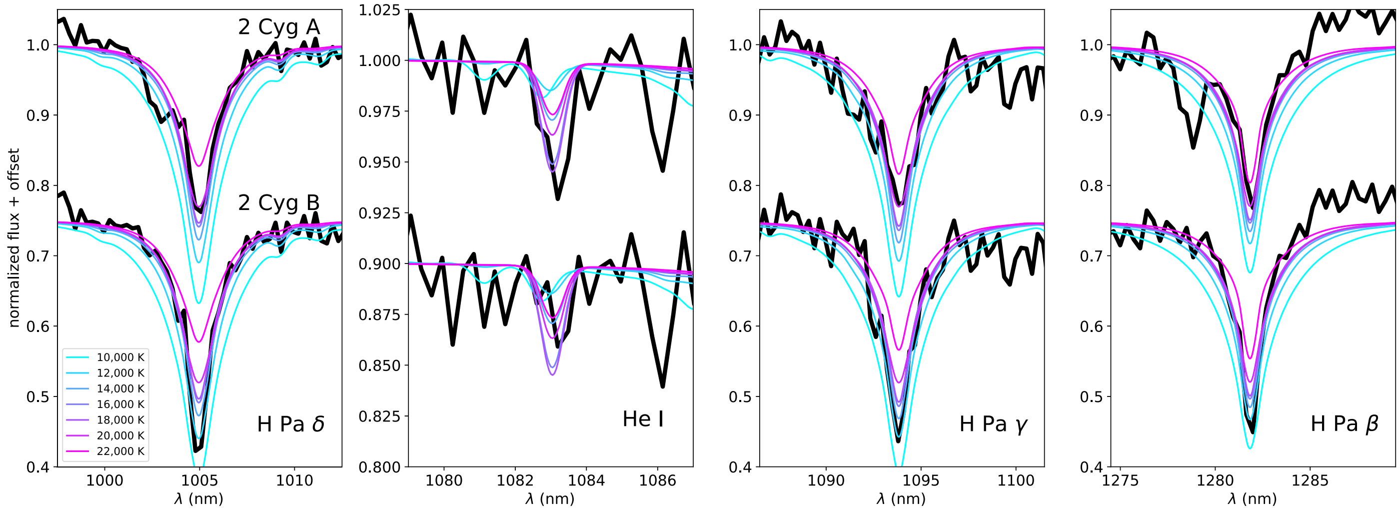

Figure 8. The NIR hydrogen Paschen line series and neutral helium compared with BT-Settl models for 2 Cygni A and 2 Cygni B. Different effective temperatures are considered in 2000 K increments assuming a surface gravity of $\log(g) = 4.0$. In each case, the absorption line depths are consistent with a lower temperature for 2 Cygni B than 2 Cygni A.

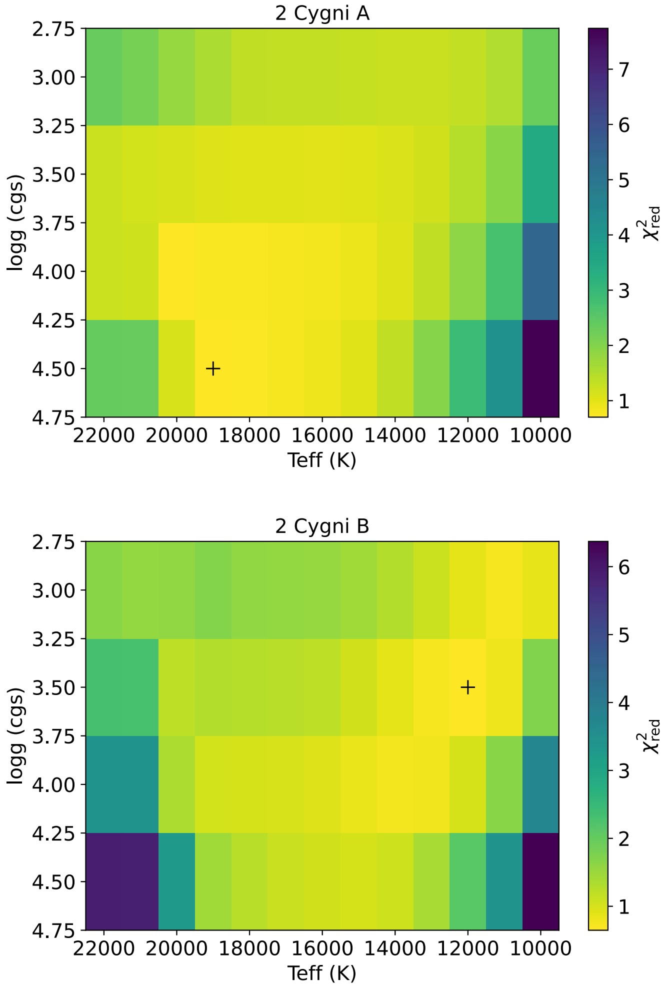

Figure 9. Grid comparisons for 2 Cygni A and B when fitting atmospheric models to the full spectrum. A plus sign indicates the location of the lowest $\chi^2_{\rm red}$ value.

wavelengths by 2 Cygni A. We can also compare the estimated effective temperatures from spectroscopy to photometry (Figure 6). For 2 Cygni A, we find excellent agreement in that the L. Girardi et al. (2002) models estimate an effective temperature of $T_{\rm A} = 18{,}800 \pm 200$ K at an age of $\log(t) = 7.55$ ($t = 35$ Myr). For 2 Cygni B, the estimated effective temperature from evolutionary models is lower, $T_{\rm B} = 17{,}700 \pm 300$ K, but lies outside of the range indicated by spectroscopic model fits. Thus, further high spatial resolution and high spectral resolution measurements are needed to resolve this tension for the companion temperature.

Finally, we attempted to measure relative RVs of each component using Lili. We find that each spectrum shares the same barycentric correction but were unable to detect an offset in Doppler velocity. At the resolution of the Lili measurements, we are able to place an upper limit of ≈±16 km $\rm s^{-1}$ on the relative RV between the sources.

The fact that 2 Cygni B appears to be a star that shares a similar spectral classification as 2 Cygni A, yet is fainter and has a lower temperature, argues against the idea of being a chance-alignment foreground or background object. If the 2 Cygni B candidate were a foreground stellar object, we would expect it to have redder colors than 2 Cygn A assuming closer distances to the Sun. Instead, 2 Cygni B has neutral colors and similar spectral type suggesting a similar distance as 2 Cygni A. If the 2 Cygni B candidate were a background stellar object, we would expect it to have different colors than 2 Cygni A, which was shown not to be the case (Section 5.1).

5.3. False-positive Analysis

We use the TRILEGAL Galactic model tool from L. Girardi et al. (2005) to estimate the number density of stars in the direction of 2 Cygni. The model includes thin disk, thick disk, and halo components. The false-positive probability of coincident line-of-site sources is estimated by considering an area of sky with radius $r = 90$ mas. Located 6° from the Galactic plane, TRILEGAL expects to find approximately 11 sources having $H < 7$ within an area of 0.5 $\rm deg^2$ centered around 2 Cygni. Assuming a uniform rate of occurrence in this region of interest, the expected number of sources located within 90 mas of 2 Cygni is $\approx 4.3 \times 10^{-8}$. Given this finding, along with the fact that the secondary has a similar color as 2 Cygni A, we conclude that the likelihood of the imaged source being an unrelated foreground or background object is low.

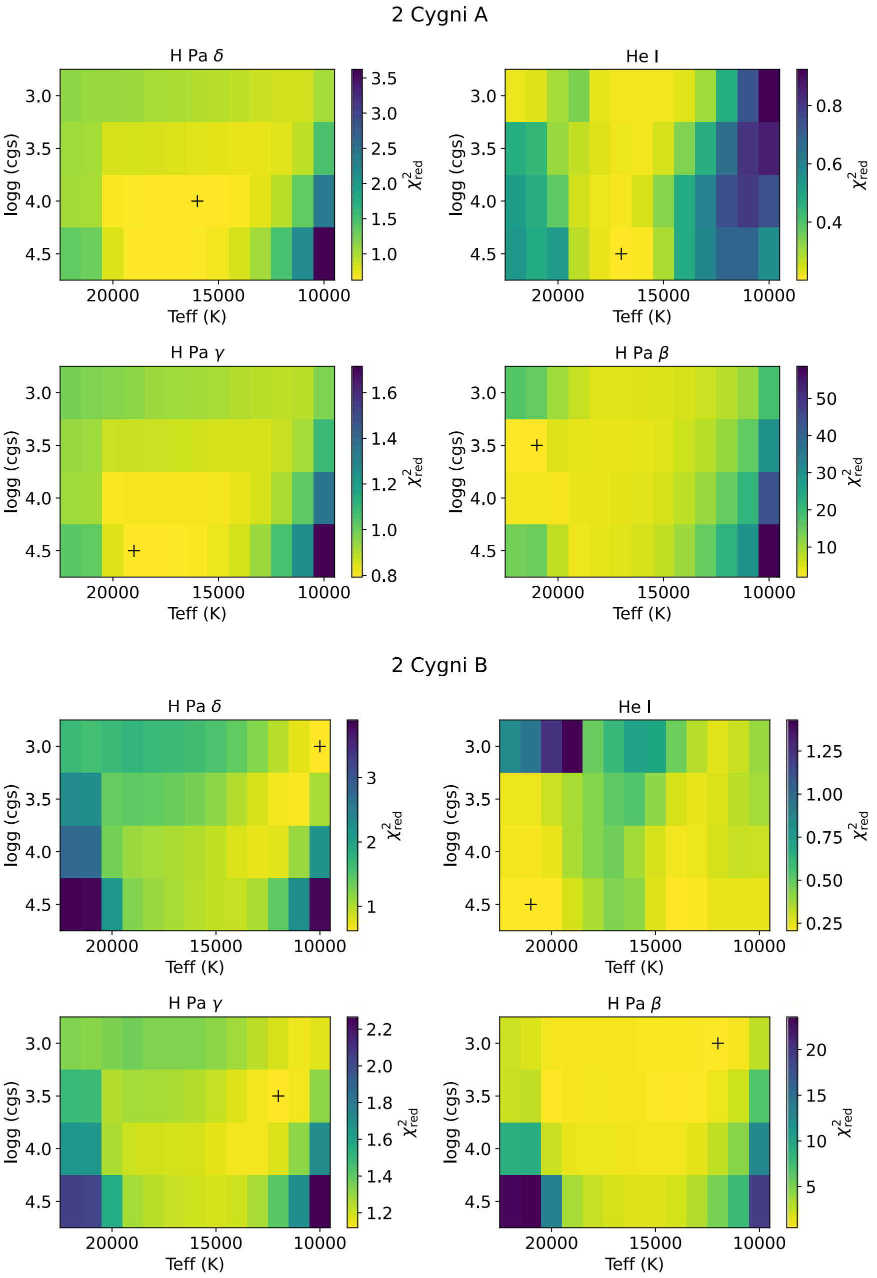

Figure 10. Grid comparisons for 2 Cygni A and B when fitting atmospheric models to individual absorption lines. A plus sign indicates the location of the lowest $\chi^2_{\rm red}$ value.

6. Summary and Concluding Remarks

The first major subsystem of the iLocater instrument, the SX acquisition camera, has been installed and commissioned at the LBT. The unit injects starlight directly into SMFs for spectroscopy in the wavelength range $\lambda = 0.97$–1.31 μm, while shorter wavelengths ($\lambda = 0.927$–0.960 μm) are diverted to a high-speed camera to record diffraction-limited images for both science and real-time diagnostics (A. J. Bechter et al. 2020; J. Crass et al. 2021a). In this paper, we demonstrate the capabilities of this newly commissioned AO instrument by reporting the serendipitous imaging discovery of a previously unknown binary star system with a separation of only $\theta = 70$ mas.

We further demonstrate the first end-to-end spectroscopic measurements using the precursor Lili spectrograph, which helped to characterize each binary star component (R. J. Harris et al. 2024). Broadband measurements at $R \approx 1500$ show a similar spectral energy distribution for each resolved star. The estimated range of effective temperatures from hydrogen absorption features suggests that 2 Cygni is comprised of an early-type B star and late-type B star.

Evidence suggesting 2 Cygni's binary nature consists of multiepoch, multiinstrument, multifilter direct imaging detection of a candidate source with relative brightness, colors, and spectrum consistent with companionship. The off-axis source can likely only be detected using AO (or possibly speckle imaging) on a large telescope. The false-positive probability of a nearby foreground or background stellar source located in such close proximity to 2 Cygni with these attributes is less than one in $23 \times 10^6 (1/4.3 \times 10^{-8})$.

Representing a bright star in the Cygnus constellation, the naked-eye ($V = 4.98$), B star 2 Cygni appears to be a massive visual binary system. Additional follow-up measurements are needed however to break degeneracies between proper motion and possible orbital motion, determining with certainty whether the candidate is a bona fide companion. If gravitationally bound, the full orbit of 2 Cygni could be reconstructed in the future with long time baseline Doppler RV measurements combined with AO imaging. Distinguishing between orbital motion and Galactic spatial motion will be important for precisely tracing the trajectory of 2 Cygni backwards in time. The detection of 2 Cygni B may impact the parallax measured by Gaia and estimated absolute magnitudes; thus system parameters will need to be updated with any refinements of the distance to 2 Cygni. Finally, it remains to be seen whether a third, more distant, source may be associated with 2 Cygni at tens of arcseconds separation as suggested by J. Dommanget & O. Nys (2002).

Nearby companions can impact the evolution of massive stars in binary systems, but only those with orbital periods less than ≈1500 days might exchange mass (H. Sana et al. 2012). The 2 Cygni components are sufficiently separated that mass exchange is unlikely to occur. Many young, massive stars are known to host a close binary companion, but the fraction depends on environment (field, cluster, runaway stars, walk-away stars, etc.; R. Chini et al. 2012). One way to produce anomalous spatial velocities is through disruption of binary systems via mass transfer, resulting in a lower number of companions; alternatively, ejection from a star cluster, e.g., through interaction with a black hole, can give rise to peculiar velocities (M. Renzo et al. 2019). Thus, studying the multiplicity and kinematics of early-type systems like 2 Cygni can help to inform Galactic formation scenarios by providing context for their evolution.

Acknowledgments

We thank the many LBTO staff and engineers for their tireless efforts in facilitating the transport, rebuild, integration, and testing of the iLocater SX acquisition camera system. This research is based upon instrumentation work supported by the National Science Foundation under grant No. 2108603. J.R. C. acknowledges support from the NASA Early Career Fellowship (NNX13AB03G) and NSF CAREER programs (1654125). This research has made use of the Washington Double Star Catalog maintained at the U.S. Naval Observatory. M.C.J. acknowledges support from the Thomas Jefferson Endowment for Space Exploration at Ohio State. This research was supported in part through a service agreement with the Notre Dame Engineering and Design Core Facility (EDCF). We thank David Futa, Matthew Sanford, and Gary Edwards from the Notre Dame physics machine shop for building custom mechanical components. We are grateful for feedback from the iLocater acquisition camera preliminary design review (PDR) and final design review (FDR) committee panel members, including Nemanja Jovanovic, Bertrand Mennesson, Chad Bender, Julian Christou, Olivier Lai, Reed Riddle, Tom McMahon, Douglas Summers, Christian Veillet, and others who offered helpful suggestions and insights that improved the instrument design. Finally, we are very grateful for the support and vision of the Potenziani family and Mr. Ted Wolfe. The LBT is an international collaboration among institutions in the United States, Italy, and Germany. LBT Corporation partners are: The University of Arizona on behalf of the Arizona university system; Istituto Nazionale di Astrofisica, Italy; LBT Beteiligungsgesellschaft, Germany, representing the Max-Planck Society, the Astrophysical Institute Potsdam, and Heidelberg University; The Ohio State University, and The Research Corporation, on behalf of The University of Notre Dame, University of Minnesota, and University of Virginia. Observations have benefited from the use of ALTA Center (alta.arcetri.inaf.it) forecasts performed with the Astro-Meso-Nh model. Initialization data of the ALTA automatic forecast system come from the General Circulation Model (HRES) of the European Centre for Medium Range Weather Forecasts.

ORCID iDs

Justin R. Crepp https://orcid.org/0000-0003-0800-0593
Jonathan Crass https://orcid.org/0000-0002-1503-2852
Andrew J. Bechter https://orcid.org/0000-0002-3047-9599
Brian L. Sands https://orcid.org/0009-0000-4650-2266
Derek Kopon https://orcid.org/0000-0003-0121-5815
Matthew Engstrom https://orcid.org/0009-0004-8248-3073
James E. Smous https://orcid.org/0009-0007-4806-3894
Eric B. Bechter https://orcid.org/0000-0001-8725-8730
Robert Harris https://orcid.org/0000-0002-8518-4640
Marshall C. Johnson https://orcid.org/0000-0002-5099-8185
Steve Ertel https://orcid.org/0000-0002-2314-7289
B. Scott Gaudi https://orcid.org/0000-0003-0395-9869
Philip Hinz https://orcid.org/0000-0002-1954-4564
Marc Kuchner https://orcid.org/0000-0002-2387-5489
Richard Pogge https://orcid.org/0000-0003-1435-3053
Christian Schwab https://orcid.org/0000-0002-4046-987X
Karl Stapelfeldt https://orcid.org/0000-0002-2805-7338
Ji Wang (王吉) https://orcid.org/0000-0002-4361-8885
Charles E. Woodward https://orcid.org/0000-0001-6567-627X

References

Allard, F., Homeier, D., & Freytag, B. 2011, in ASP Conf. Ser. 448, 16th Cambridge Workshop on Cool Stars, Stellar Systems, and the Sun, ed. C. M. Johns-Krull (San Francisco, CA: ASP), 91
Bechter, A., Crass, J., Ketterer, R., et al. 2016, Proc. SPIE, 9909, 99092X
Bechter, A. J., Bechter, E. B., Crepp, J. R., et al. 2020, PASP, 132, 095001
Bechter, A. J., Crass, J., Tesch, J., et al. 2020, PASP, 132, 015001
Bechter, E. B., Bechter, A. J., Crepp, J. R., et al. 2019a, PASP, 131, 024504
Bechter, E. B., Bechter, A. J., Crepp, J. R., et al. 2019b, JATIS, 5, 038004
Bechter, E. B., Bechter, A. J., Crepp, J. R., et al. 2021, JATIS, 7, 035008
Bechter, E. B., Crepp, J. R., Ngo, H., et al. 2014, ApJ, 788, 2
Blaauw, A. 1961, BAN, 15, 265
Borucki, W. J., Agol, E., Fressin, F., et al. 2013, Sci, 340, 587
Cegla, H. M., Shelyag, S., Watson, C. A., et al. 2013, ApJ, 763, 95
Cegla, H. M., Watson, C. A., Shelyag, S., et al. 2018, ApJ, 866, 55
Cegla, H. M., Watson, C. A., Shelyag, S., et al. 2019, ApJ, 879, 55
Chini, R., Hoffmeister, V. H., Nasseri, A., et al. 2012, MNRAS, 424, 1925
Ciardi, D. R., Fabrycky, D. C., Ford, E. B., et al. 2013, ApJ, 763, 41
Crass, J., Aikens, D., Mason, J., et al. 2022, Proc. SPIE, 12184, 121841P
Crass, J., Bechter, A., Sands, B., et al. 2021a, MNRAS, 501, 2250
Crass, J., Gaudi, B. S., Leifer, S., et al. 2021b, arXiv:2107.14291
Crepp, J. R. 2014, Sci, 346, 809
Crepp, J. R., Crass, J., King, D., et al. 2016, Proc. SPIE, 9908, 990819
Crepp, J. R., Johnson, J. A., Howard, A. W., et al. 2012, ApJ, 761, 39
Crepp, J. R., Johnson, J. A., Howard, A. W., et al. 2013, ApJ, 774, 1
Crepp, J. R., Johnson, J. A., Howard, A. W., et al. 2014, ApJ, 781, 29
Crepp, J. R., Pueyo, L., Brenner, D., et al. 2011, ApJ, 729, 132
Cutri, R. M., Skrutskie, M. F., van Dyk, S., et al. 2003, The IRSA 2MASS All-Sky Point Source Catalog (Washington, DC: NASA)
Davis, A. B., Cisewski, J., Dumusque, X., et al. 2017, ApJ, 846, 59
Dommanget, J., & Nys, O. 2002, yCat, I/274
Dumusque, X. 2018, A&A, 620, A47
Dumusque, X., Boisse, I., & Santos, N. C. 2014, ApJ, 796, 132

Eastman, J. D., Beatty, T. G., Siverd, R. J., et al. 2016, AJ, 151, 45

Eggleton, P. P., & Tokovinin, A. A. 2008, MNRAS, 389, 869

Fischer, D. A., Anglada-Escude, G., Arriagada, P., et al. 2016, PASP, 128, 066001

Gaia Collaboration, Smart, R. L., Sarro, L. M., et al. 2021, A&A, 649, A6

Gelman, A., & Rubin, D. B. 1992, StaSc, 7, 457

Girardi, L., Bertelli, G., Bressan, A., et al. 2002, A&A, 391, 195

Girardi, L., Groenewegen, M. A. T., Hatziminaoglou, E., et al. 2005, A&A, 436, 895

Gray, R. O., & Corbally, C. J. 1994, AJ, 107, 742

Guizar-Sicairos, M., Thurman, S. T., & Fienup, J. R. 2008, OptL, 33, 156

Gullikson, K., Kraus, A., & Dodson-Robinson, S. 2016, AJ, 152, 40

Harris, R. J., Johnson, J. C. M. C., Bechter, A., et al. 2024, MNRAS, in press

Hastings, W. K. 1970, Biometrika, 57, 97

Hinz, P. M., Defrère, D., Skemer, A., et al. 2016, Proc. SPIE, 9907, 990704

Hoffleit, D., & Jaschek, C. 1991, The Bright Star Catalogue (New Haven, CT: Yale Univ. Observatory)

Høg, E., Fabricius, C., Makarov, V. V., et al. 2000, A&A, 355, L27

Horne, K. 1986, PASP, 98, 609

Howell, S. B., Rowe, J. F., Bryson, S. T., et al. 2012, ApJ, 123, 746

Makarov, V. V., & Kaplan, G. H. 2005, AJ, 129, 2420

Marois, C., Macintosh, B., Barman, T., et al. 2008, Sci, 322, 1348

Metropolis, N., Rosenbluth, A. W., Rosenbluth, M. N., et al. 1953, JChPh, 21, 1087

Moe, M., & Di Stefano, R. 2017, ApJS, 230, 15

Moe, M., Kratter, K. M., & Badenes, C. 2019, ApJ, 875, 61

Morton, T. D., Bryson, S. T., Coughlin, J. L., et al. 2016, ApJ, 822, 86

Offner, S. S. R., Moe, M., Kratter, K. M., et al. 2023, in ASP Conf. Ser. 534, Protostars and Planets VII, ed. S.-I. Inutsuka (San Francisco, CA: ASP), 275

Perryman, M. A. C., Lindegren, L., Kovalevsky, J., et al. 1997, A&A, 500, 501

Pinna, E., Esposito, S., Hinz, P., et al. 2016, Proc. SPIE, 9909, 99093V

Plavchan, P., Latham, D., Gaudi, S., et al. 2015, arXiv:1503.01770

Poveda, A., Ruiz, J., & Allen, C. 1967, BOTT, 4, 86

Pueyo, L., Crepp, J. R., Vasisht, G., et al. 2012, ApJS, 199, 6

Renzo, M., Zapartas, E., de Mink, S. E., et al. 2019, A&A, 624, A66

Ricker, G. R., Winn, J. N., Vanderspek, R., et al. 2015, JATIS, 1, 014003

Reed, B. C. 2003, AJ, 125, 2531

Robertson, J. G., & Bland-Hawthorn, J. 2012, Proc. SPIE, 8446, 844623

Sana, H., de Mink, S. E., de Koter, A., et al. 2012, Sci, 337, 444

Schwab, C., Leon-Saval, S. G., Betters, C. H., et al. 2012, arXiv:1212.4867

Schwamb, M. E., Orosz, J. A., Carter, J. A., et al. 2013, ApJ, 768, 127

Strassmeier, K. G., Ilyin, I., Järvinen, A., et al. 2015, AN, 336, 324

Swihart, S. J., Garcia, E. V., Stassun, K. G., et al. 2017, AJ, 153, 16

Tetzlaff, N., Neuhäuser, R., & Hohle, M. M. 2011, MNRAS, 410, 190

Turon, C., Creze, M., Egret, D., et al. 1993, BICDS, 43, 5

van Leeuwen, F. 2007, A&A, 474, 653

Wielen, R., Schwan, H., Dettbarn, C., et al. 2000, VeARI, 37, 1

Worley, C. E. 1978, PUSNO, 24, 1

Worley, C. E., & Douglass, G. G. 1997, A&AS, 125, 523

Wilson, R. H. 1950, AJ, 55, 153

Wright, J. T., Roy, A., Mahadevan, S., et al. 2013, ApJ, 770, 119